Chemistry & Biology
Article

Distinct Structural Elements Dictate the Specificity of the Type III Pentaketide Synthase from *Neurospora crassa*

Sheryl B. Rubin-Pitel,[1,5] Houjin Zhang,[2,5] Trang Vu,[1] Joseph S. Brunzelle,[3] Huimin Zhao,[1,2,4,*] and Satish K. Nair[2,4,*]
[1]Department of Chemical and Biomolecular Engineering
[2]Department of Biochemistry
University of Illinois at Urbana-Champaign, 600 S. Mathews Avenue, Urbana, IL 61801, USA
[3]Life Sciences Collaborative Access Team, Argonne National Laboratories, Argonne, IL 60439, USA
[4]Center for Biophysics and Computational Biology, University of Illinois at Urbana-Champaign, 600 S. Mathews Avenue, Urbana, IL 61801, USA
[5]These authors contributed equally to this work
*Correspondence: zhao5@uiuc.edu (H.Z.), snair@uiuc.edu (S.K.N.)
DOI 10.1016/j.chembiol.2008.08.011

SUMMARY

The fungal type III polyketide synthase 2′-oxoalkylresorcylic acid synthase (ORAS) primes with a range of acyl-Coenzyme A thioesters (C_4–C_{20}) and extends using malonyl-Coenzyme A to produce pyrones, resorcinols, and resorcylic acids. To gain insight into this unusual substrate specificity and product profile, we have determined the crystal structures of ORAS to 1.75 Å resolution, the Phe-252→Gly site-directed mutant to 2.1 Å resolution, and a binary complex of ORAS with eicosanoic acid to 2.0 Å resolution. The structures reveal a distinct rearrangement of structural elements near the active site that allows accommodation of long-chain fatty acid esters and a reorientation of the gating mechanism that controls cyclization and polyketide chain length. The roles of these structural elements are further elucidated by characterization of various structure-based site-directed variants. These studies establish an unexpected plasticity to the PKS fold, unanticipated from structural studies of other members of this enzyme family.

INTRODUCTION

Polyketides, a diverse class of secondary metabolites with antibacterial and antitumor activity, are synthesized by polyketide synthases (PKSs), a family of enzymes and multienzyme complexes nearly as varied as the products they create (Austin and Noel, 2003; Watanabe et al., 2007). In contrast to type I and type II PKSs, which are large multidomain enzymes or multisubunit complexes, respectively, type III polyketide synthases are self-contained homodimeric enzymes, where the single active site in each monomer iteratively catalyzes the priming, extension, and cyclization reactions needed to create a polyketide product (Jez et al., 2001). In spite of their structural simplicity, type III PKSs produce a wide array of compounds, including pyrones, acridones, chalcones, stilbenes, and phloroglucinols (Schröder, 1999) (Figure 1). The multiplicity of products hinges on the ability of type III PKSs to utilize a variety of acyl-CoA thioesters for priming, to extend with varying numbers of malonyl-CoA units, and also to cyclize the linear polyketide intermediate by any of several condensation reactions. Whereas type III PKSs from plants such as chalcone and stilbene synthase have been studied for many years, members of this family were recognized in bacteria more recently, and the first characterization of a fungal type III PKS was reported in 2007 (Funa et al., 2007).

Filamentous fungi produce a variety of polyketide compounds, representatives of which are both highly toxic (aflatoxin) and pharmacologically useful (lovastatin). The known polyketide products of filamentous fungi have thus far been traced to the activity of type I PKSs (Cox, 2007), but putative type III PKSs have also been uncovered by analyzing the recently sequenced genomes of organisms including *Aspergillus oryzae*, *Magnaporthe grisea*, and *Neurospora crassa* (Seshime et al., 2005). The product of *N. crassa* open reading frame NCU04801.1 was recently confirmed to be a type III PKS which prefers long-chain acyl-CoAs for priming, carries out extension using malonyl-CoA, and produces pyrone, resorcinol, and resorcylic acid products (Funa et al., 2007). Product profile analysis of this open reading frame identifies the pentaketide resorcylic acid 2′-oxoalkylresorcylic acid as the major product, and this enzyme was named 2′-oxoalkylresorcylic acid synthase (ORAS). ORAS is one of several known type III PKSs to use long-chain acyl-CoA substrates and produces tetraketide and pentaketide resorcylic acids using C_{16}, C_{18}, and C_{20} CoA esters as starter units (Funa et al., 2007). Alignment of ORAS and other type III PKSs of plant and bacterial origin reveals a carboxy-terminal extension of approximately 50 residues beyond similar enzymes (see Figure S1 available online), and ORAS is longer than the only other type III PKS known to have a carboxy-terminal extension, 1,3,6,8-tetrahydroxynaphthalene synthase (THNS) from *Streptomyces coelicolor* (Izumikawa et al., 2003).

Structural analysis of *Medicago sativa* chalcone synthase (CHS) (Ferrer et al., 1999), *Pinus sylvestris* stilbene synthase (STS) (Austin et al., 2004a), *Gerbera hybrida* 2-pyrone synthase (2PS) (Jez et al., 2000), and *Aloe arborescens* pentaketide chromone synthase (PCS) (Morita et al., 2007) from plants, and of the bacterial enzymes *Mycobacterium tuberculosis* Pks18 (Sankaranarayanan

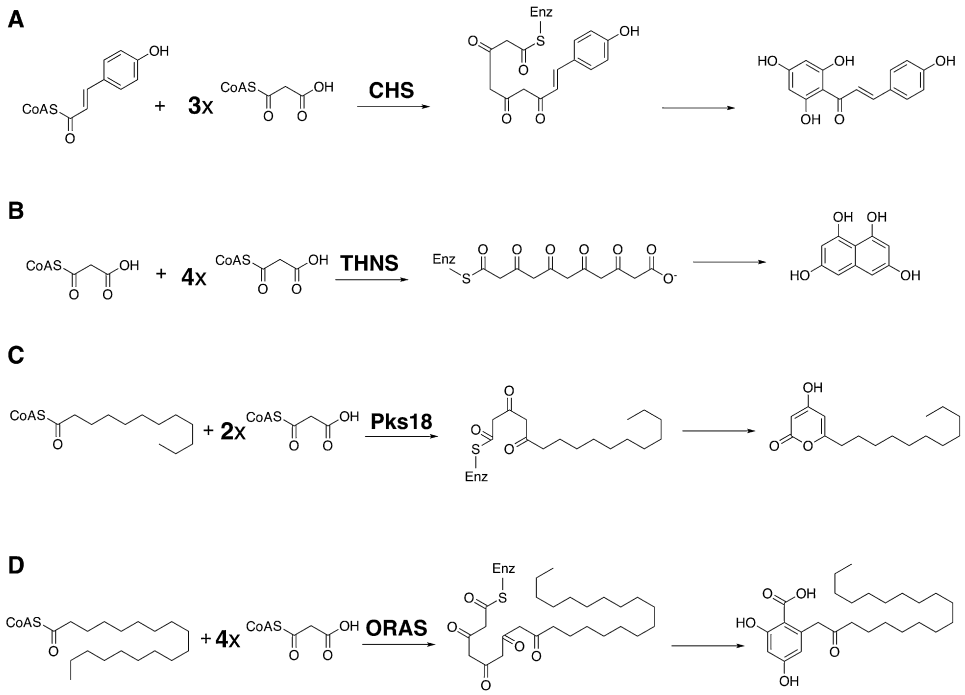

Figure 1. Reaction Schemes of the Synthesis of Polyketides

(A) Naringenin chalcone synthesized from 4-coumaroyl-CoA and three molecules of malonyl-CoA by *M. sativa* CHS.

(B) 1,3,6,8-tetrahydroxynaphthalene synthesized from five molecules of malonyl-CoA by *S. coelicolor* THNS.

(C) Myristoyl triketide pyrone synthesized from one molecule of lauroyl-CoA and two molecules of malonyl-CoA by *M. tuberculosis* Pks18.

(D) Stearoyl pentaketide resorcylic acid synthesized from stearoyl-CoA and four molecules of malonyl-CoA by *N. crassa* ORAS. Enzymatic decarboxylation of resorcylic acid results in the production of the product resorcinol.

et al., 2004) and *S. coelicolor* THNS (Austin et al., 2004b) have provided useful insight into the basis of starter molecule specificity and mechanism of biosynthesis (Figure 1). Although these enzymes share common core architectural features, subtle rearrangements of the polypeptide main chain and alteration of critical residues at the active site result in the functional diversity of the type III polyketide synthases. In order to elucidate the structural basis for long-chain starter molecule specificity and gain insights into the mechanism of pentaketide alkylresorcylic acid synthesis, we have determined the crystal structures of a fully active truncation variant of ORAS to 1.76 Å resolution, of the Phe-252→Gly site-directed mutant to 2.1 Å resolution, and of a binary complex of truncated ORAS with eicosanoic acid (a C_{20} fatty acid) to 2.0 Å resolution. The crystal structures reveal a distinct rearrangement of structural elements near the enzyme active site that allows for accommodation of long-chain fatty acid esters and unique active site features that result in a reorientation of the gating mechanism for controlling cyclization pattern and polyketide chain length. These structures reveal an unexpected static nature of the acyl-binding tunnel and suggest mechanistic similarities to bacterial type III polyketide synthases (Sankaranarayanan et al., 2004).

RESULTS

Expression of His-Tagged ORAS in *Escherichia coli*

The ORAS-encoding open reading frame NCU04801.1 was amplified from a library of *N. crassa* mRNA and initially cloned with an amino-terminal hexahistidine affinity tag. The purified recombinant protein was heterogeneous as judged by SDS-PAGE analysis due to degradation of the carboxy terminus. Consequently, the ORAS gene product was recloned with a carboxy-terminal hexahistidine tag preceded by a thrombin cleavage site. To determine whether the 50 residue carboxy-terminal extension, observed upon alignment of ORAS with other type III PKS enzymes, is necessary for catalysis, a truncated mutant with a deletion of this extension (trORAS) was generated.

In Vitro Analysis of Recombinant ORAS

The steady-state kinetic parameters of trORAS and ORAS were determined for the priming substrate stearoyl-CoA from initial velocity measurements of the formation of free CoASH. Results for recombinant ORAS (K_m = 3.9 μM and k_{cat} = 6.7 × 10^{-4} s^{-1}) and trORAS (K_m = 3.5 μM and k_{cat} = 6.3 × 10^{-4} s^{-1}) are quite similar, indicating that the carboxy-terminal extension is not required for enzymatic activity. Our results reflect similar findings obtained for a 25 residue carboxy-terminal truncated variant of *S. coelicolor* THNS (see Figure S1), which was shown to possess activity similar to that of the wild-type enzyme (Austin et al., 2004b). Additional comparison of the specific activity and product profile for trORAS and ORAS is provided in Figure S3.

Structural Rearrangements in the Lower Domain of ORAS

Crystallization attempts of full-length ORAS were hampered by the propensity of the enzyme to degrade over the course of

Table 1. Data Collection, Phasing, and Refinement Statistics

	Native ORAS	SeMet ORAS	F252G ORAS	Eicosanoic Acid
Data Collection				
Space group	$P2_12_12_1$	$P2_12_12_1$	$P2_1$	$P2_1$
Unit cell dimensions				
a, *b*, *c* (Å)	69.7, 105.0, 105.3	68.5, 103.0, 105.6	69.7, 105.1, 105.1	68.9, 105.9, 104.1
α, β, γ (°)	90.0, 90.0, 90.0	90.0, 90.0, 90.0	90.0, 90.3, 90.0	90.0, 90.1, 90.0
Resolution (Å)[a]	50–1.75 (1.86–1.75)	50–2.2 (2.28–2.2)	50–2.1 (2.18–2.1)	50–2.0 (2.07–2.0)
R_{sym} (%)[b]	11.2 (56.2)	6.5 (17.9)	7.1 (29.3)	8.1 (29.1)
I/σ (I)	11.3 (2.9)	37.1 (8.9)	17.2 (3.3)	16.4 (4.8)
Completeness (%)	97.9 (92.4)	98.1 (97.5)	96.3 (90.1)	97.0 (88.7)
Redundancy	6.5 (5.7)	5.3 (5.1)	3.3 (2.8)	4.3 (3.9)
$\|F_H\|/\varepsilon$ (centric/acentric)		1.859		
FOM/DM FOM[c]		42.52/69.58		
Refinement				
Resolution (Å)	25.0–1.75		25.0–2.1	25.0–2.0
Number of reflections	74,247		80,720	92,963
R_{work}/R_{free}[d]	17.9/20.9		19.8/25.6	17.4/22.5
Number of atoms				
Protein	5,698		11,368	11,396
Solvent	733		824	805
PEG	0		38	0
Eicosanoic acid	0		0	44
Average B value				
Protein	17.6		27.8	30.3
Solvent	29.1		30.3	38.9
Ligand			43.0	50.4
Rms deviations				
Bond lengths (Å)	1.16		1.29	1.19
Bond angles (°)	0.008		0.010	0.012

[a] Highest resolution shell is shown in parentheses.
[b] $R_{sym} = \Sigma|(I_i - < I_i >)|\Sigma I_i$, where I_i = intensity of the *i*th reflection and $< I_i >$ = mean intensity.
[c] Mean figure of merit before and after density modification.
[d] R factor = $\Sigma(|F_{obs}| - k|F_{calc}|)/\Sigma|F_{obs}|$ and R free is the R value for a test set of reflections consisting of a random 5% of the diffraction data not used in the refinement.

a few hours following purification. Mass spectrometric analysis of the degradation product suggested cleavage at residues located at the charged carboxy-terminal extension. Limited proteolysis confirmed that the residues at the carboxy terminus are labile and, as the variant lacking carboxy-terminal extension residues is shown to be fully catalytically competent, crystallization efforts were focused on this deletion variant.

Screening of this truncated ORAS readily produced crystals utilizing polyethylene glycol 8000 as a precipitant. As attempts to solve the structure of trORAS by molecular replacement using the coordinates of other type III polyketide synthases were not successful, crystallographic phases were determined de novo using single-wavelength anomalous scattering from crystals grown from selenomethionine-incorporated protein. The resultant electron density map was of exceptional quality, permitting a trace of all residues from Ala-9 through Arg-388 in each monomer and refinement against a 1.75 Å resolution data set to a final R factor/free R factor of 17.9%/20.8% (see Table 1 for further details).

The overall structure of trORAS recapitulates the characteristic bidomain fold observed in structures of other type III polyketide synthases (Jez et al., 2001), albeit with novel distinguishing structural elements (Figure 2A). A structure-based similarity search using the Dali search engine (Holm and Sander, 1995) queried against the Protein Data Bank (Berman et al., 2000) identifies chalcone synthase (Ferrer et al., 1999) as the closest structural homolog (Z score = 46.9, root-mean-square deviation [rmsd] of 2.2 Å over 355 residues aligned with a sequence identity of 24%). Two other homologs of note, which share a significant characteristic structural feature with ORAS (see below), are the bacterial type III PKS enzymes, particularly *S. coelicolor* THNS (Austin et al., 2004b) (Z score = 42.8, rmsd of 2.3 Å over 344 residues aligned with a sequence identity of 24%), and *M. tuberculosis* Pks18 (Sankaranarayanan et al., 2004) (Z score = 44.2, rmsd of 2.2 Å over 346 residues aligned with a sequence identity of 24%) (see Figure 2B for a structure-based sequence alignment).

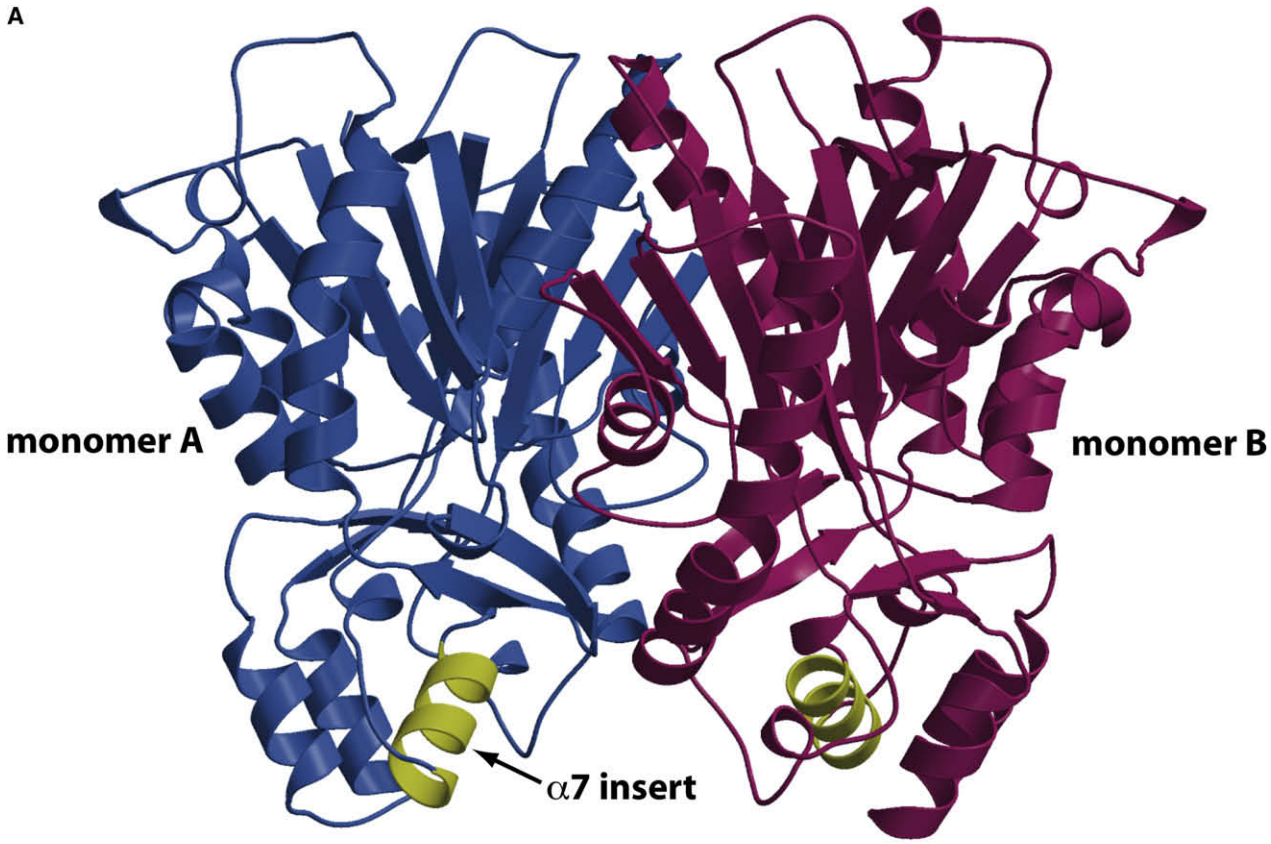
A
monomer A
monomer B
α7 insert

B

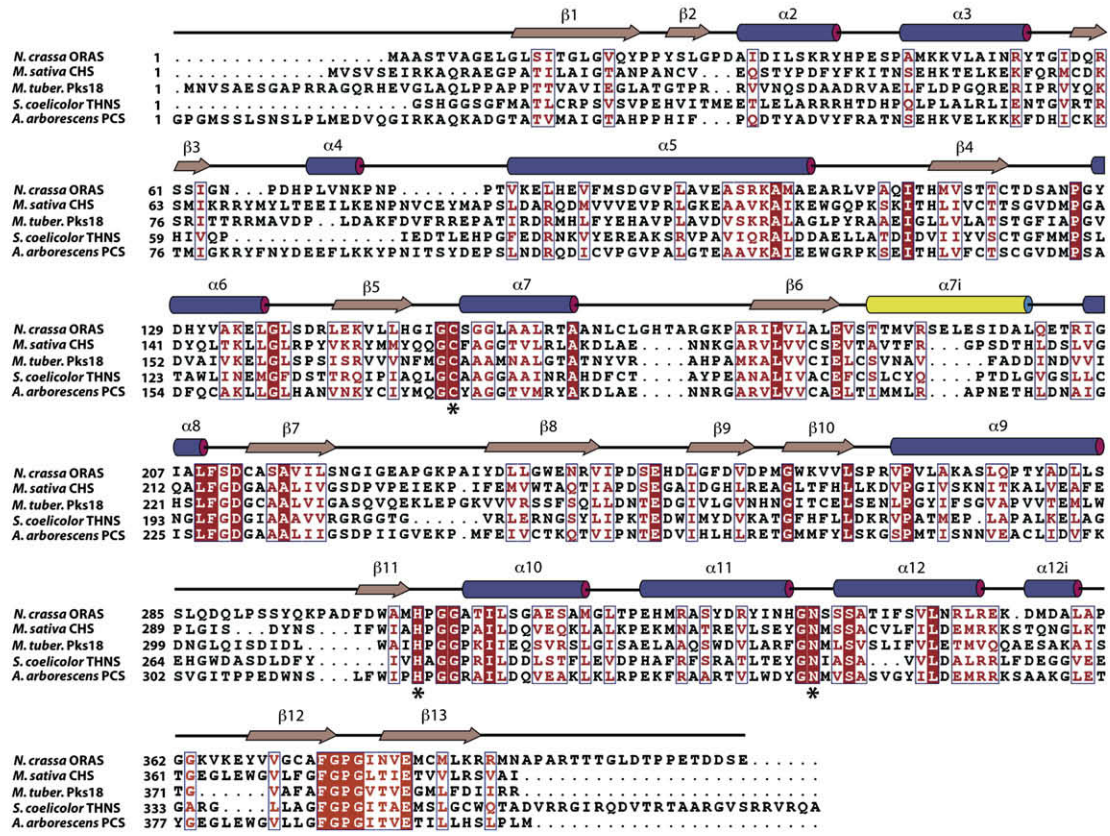
β1 β2 α2 α3
N. crassa ORAS 1 . . . . . MAASTVAGELGLSITGLGVQYPPYSLGPDAIDILSKRYHPESPAMKKVLAINRYTGIDQR
M. sativa CHS 1 . . . . . MVSVSEIRKAQRAEGPATILAIGTANPANCV . . EQSTYPDFYFKITNSEHKTELKEKFQRMCDK
M. tuber. Pks18 1 . MNVSAESGAPRRAGQRHEVGLAQLPPAPPTTVAVIEGLATGTPR . . RVVNQSDAADRVAELFLDPGQRERIPRVVQK
S. coelicolor THNS 1 . . . . . GSHGGSGFMATLCRPSVSVPEHVITMEETLELARRRHTDHPQLPLALRLIENTGVRTR
A. arborescens PCS 1 GPGMSSLSNSLPLMEDVQGIRKAQKADGTATVMAIGTAHPPHIF . . . PQDTYADVYFRATNSEHKVELKKKFDHICKK
β3 α4 α5 β4
N. crassa ORAS 61 SSIGN . . . PDHPLVNKPNP . . . . . PTVKELHEVFMSDGVPLAVEASRKAMAEARLVPAQITHMVSTTCTDSANPGY
M. sativa CHS 63 SMIKRRYMYLTEEILKENPNVCEYMAPSLDARQDMVVVEVPRLGKEAAVKAIKEWGQPKSKITHLIVCTTSGVDMPGA
M. tuber. Pks18 76 SRITTRRMAVDP . . LDAKFDVFRREPATIRDRMHLFYEHAVPLAVDVSKRALAGLPYRAAEIGLLVLATSTGFIAPGV
S. coelicolor THNS 59 HIVQP . . . . . IEDTLEHPGFEDRNKVYEREAKSRVPAVIQRALDDAELLATDIDVIIYVSCTGFMMPSL
A. arborescens PCS 76 TMIGKRYFNYDEEFLKKYPNITSYDEPSLNDRQDICVPGVPALGTEAAVKAIEEWGRPKSEITHLVFCTSCGVDMPSA
α6 β5 α7 β6 α7i
N. crassa ORAS 129 DHYVAKELGLSDRLEKVLLHGIGCSGGLAALRTAANLCLGHTARGKPARILVLALEVSTTMVRSELESIDALQETRIG
M. sativa CHS 141 DYQLTKLLGLRPYVKRYMMYQQGCFAGGTVLRLAKDLAE . . . . NNKGARVLVVCSEVTAVTFR . . . GPSDTHLDSLVG
M. tuber. Pks18 152 DVAIVKELGLSPSISRVVVNFMGCAAAMNALGTATNYVR . . . . AHPAMKALVVCIELCSVNAV . . . . . FADDINDVVI
S. coelicolor THNS 123 TAWLINEMGFDSTTRQIPIAQLGCAAGGAAINRAHDFCT . . . . AYPEANALIVACEFCSLCYQ . . . . PTDLGVGSLLC
A. arborescens PCS 154 DFQCAKLLGLHANVNKYCIYMQGCYAGGTVMRYAKDLAE . . . . NNRGARVLVVCAELTIMMLR . . . APNETHLDNAIG
α8 β7 β8 β9 β10 α9
N. crassa ORAS 207 IALFSDCASAVILSNGIGEAPGKPAIYDLLGWENRVIPDSEHDLGFDVDPMGWKVVLSPRVPVLAKASLQPTYADLLS
M. sativa CHS 212 QALFGDGAAALIVGSDPVPEIEKP . IFEMVWTAQTIAPDSEGAIDGHLREAGLTFHLLKDVPGISVSKNITKALVEAFE
M. tuber. Pks18 221 HSLFGDGCAALVIGASQVQEKLEPGKVVVRSSFSQLLDNTEDGIVLGVNHNGITCELSENLPGYIFSGVAPVVTEMLW
S. coelicolor THNS 193 NGLFGDGIAAAVVRGRGGTG . . . . . VRLERNGSYLIPKTEDWIMYDVKATGFHFLLDKRVPATMEP . LAPALKELAG
A. arborescens PCS 225 ISLFGDGAAALIIGSDPIIGVEKP . MFEIVCTKQTVIPNTEDVIHLHLRETGMMFYLSKGSPMTISNNVEACLIDVFK
β11 α10 α11 α12 α12i
N. crassa ORAS 285 SLQDQLPSSYQKPADFDWAMHPGGATILSGAESAMGLTPEHMRASYDRYINHGNSSSATIFSVLNRLREK . DMDALAP
M. sativa CHS 289 PLGIS . . . DYNS . . . IFWIAHPGGPAILDQVEQKLALKPEKMNATREVLSEYGNMSSACVLFILDEMRKKSTQNGLKT
M. tuber. Pks18 299 DNGLQISDIDL . . . . . WAIHPGGPKIIEQSVRSLGISAELAAQSWDVLARFGNMLSVSLIFVLETMVQQAESAKAIS
S. coelicolor THNS 264 EHGWDASDLDFY . . . . . IVHAGGPRILDDLSTFLEVDPHAFRFSRATLTEYGNIASA . . . VVLDALRRLFDEGGVEE
A. arborescens PCS 302 SVGITPPEDWNS . . . LFWIPHPGGRAILDQVEAKLKLRPEKFRAARTVLWDYGNMVSASVGYILDEMRRKSAAKGLET
β12 β13
N. crassa ORAS 362 GGKVKEYVVGCAFGPGINVEMCMLKRRMNAPARTTTGLDTPPETDDSE . . . . . .
M. sativa CHS 361 TGEGLEWGVLFGFGPGLTIETVVLRSVAI . . . . . .
M. tuber. Pks18 371 TG . . . . . VAFAFGPGVTVEGMLFDIIRR . . . . . .
S. coelicolor THNS 333 GARG . . . . LLAGFGPGITAEMSLGCWQTADVRRGIRQDVTRTAARGVSRRVRQA
A. arborescens PCS 377 YGEGLEWGVLLGFGPGITVETILLHSLPLM . . . . . .

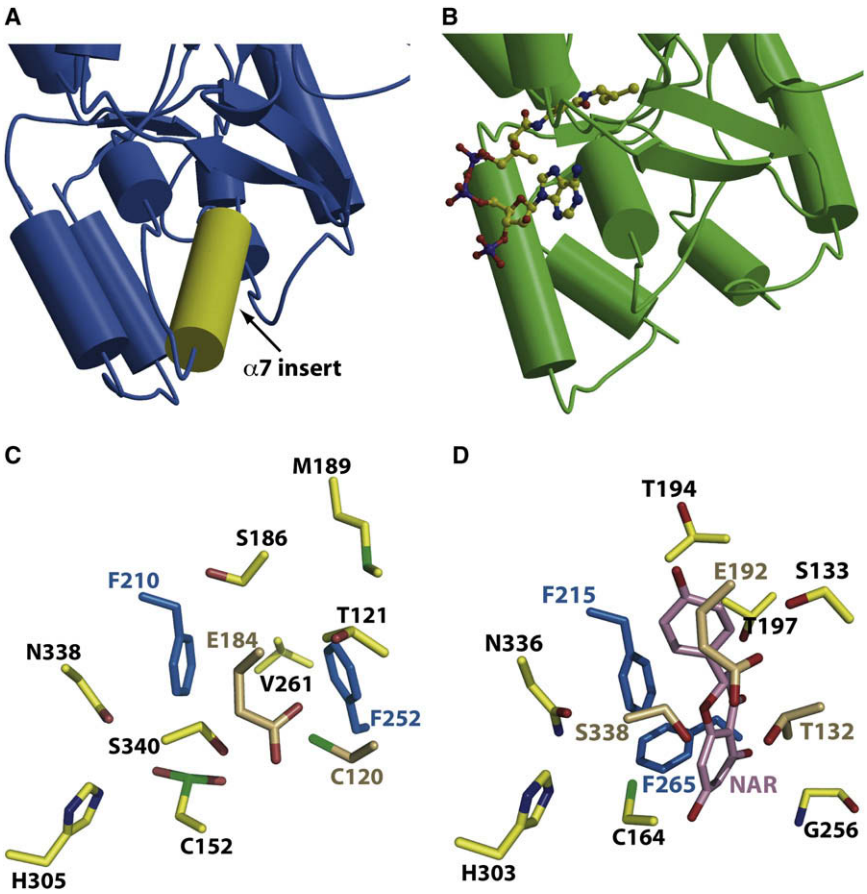

Figure 3. Close-Up View of the Active Site of trORAS

(A and B) Ribbon diagram of the lower domains of (A) ORAS in blue and (B) CHS in green with bound malonyl-CoA (shown in ball-and-stick representation) highlighting the topological differences in this region of the active site. The α7 insertion present in ORAS is shown in yellow.

(C and D) Stick-figure representations of residues that are believed to be involved in catalysis and product/substrate specificity in the active sites of (C) ORAS and (D) CHS complexed with naringenin. The phenylalanine residues that function as steric gates to control specificity are colored in blue, and residues that are implicated in participating in mechanistic steering of intermediates are shown in orange.

Although the core structure of trORAS is characteristic of that of other type III PKSs, the structure is set apart by significant deviations in the backbone relative to other enzymes of this family. The core αβαβα thiolase fold observed in the upper domains of type III PKS molecules is retained in the structure of trORAS, albeit with uncharacteristically long loop regions that vary in length in comparison with the closest structural homologs. Within one such loop region, the polypeptide backbone between α helix α12 and β sheet β12 adopts an α-helical configuration spanning residues Asp-355 through Leu-359.

The fold of the lower domain of trORAS, harboring the traditional "floor" of the type III PKS active site and containing residues that are thought to be critical for substrate and product specificities, is significantly different from that observed in other family members. Most notably, in comparisons with the structures of other type III PKSs, the loop that bridges helices α4 and α5 is shortened by about six amino acids, resulting in a depression at this juncture of the polypeptide fold. This shorter loop is compensated by an extension of residues Thr-188 through Gln-201 into the corresponding void. Unexpectedly, in this region, residues Met-189 through Asp-198 form an α-helical insertion that bridges sheets β6 and helix α8 (Figures 3A and 3B). This novel structural element, which we term insertion α7i, has not to our knowledge been previously observed in any type III PKS enzyme. In order to compensate for this helical insertion, the helix that follows this insertion (α8) and typically spans nine residues (Leu-206 through Leu-214 in *M. sativa* CHS) (Ferrer et al., 1999) has been shortened to encompass only four residues in trORAS (Gly-206 through Leu-209) (Figures 3A and 3B). These novel structural elements result in a rearrangement of the lower domain at the floor of the active site, and the functional ramifications of this rearrangement are discussed below.

Active Site Architecture

As observed in crystal structures of related type III PKS enzymes, trORAS exists as an obligate homodimer and, upon dimerization, each monomer buries 2364 Å^2 of surface area. However, trORAS lacks the amino-terminal helical extension that crosses over between the two monomeric units as in the structures of *M. sativa* CHS (Ferrer et al., 1999) and *A. arborescens* PCS (Morita et al., 2007). In addition, trORAS lacks the Met-137 residue of *M. sativa* CHS that is highly conserved in plant type III PKS and participates in intersubunit contacts by protruding into the neighboring monomer to complete the composite active site. Instead, an asparagine residue (Asn-125) is located at the equivalent position, resulting in a lack of cross-subunit interactions in the formation of the active site cavity. The opening at the active site that is required for the intersubunit

Figure 2. Overall Structure of trORAS and Multiple Sequence Alignment

(A) Ribbon diagram derived from the crystal structure of trORAS, with one monomer colored in blue and the other colored in magenta. In the lower domain of each monomer, residues Met-189 through Asp-198 form an α-helical insertion that bridges sheets β6 and helix α8. This novel structural element, which has not to our knowledge been previously observed in any type III PKS enzyme, is termed insertion α7i and is shown in yellow.

(B) Structure-based sequence alignment of ORAS with other bacterial and plant type III polyketide synthases of note, including *M. sativa* CHS, *M. tuberculosis* Pks18, *S. coelicolor* THNS, and *A. arborescens* PCS. Residues that constitute the catalytic triad are shown with an asterisk.

protrusion of Met-137 in *M. sativa* CHS is occluded in trORAS by a reorganization of the backbone between His-148 and Cys-152. A similar situation is observed in the structure of *M. tuberculosis* Pks18 that contains Ala-148 at the equivalent position and a substitution of the glycine residue at the opening by a leucine that similarly occludes cross-subunit interactions (Sankaranarayanan et al., 2004).

The catalytic triad, consisting of Cys-152, His-305, and Asn-338, is situated at a location and orientation similar to that observed in other related type III PKS enzymes (Figures 3C and 3D). Mutation of Cys-152 to threonine was performed on the truncated ORAS enzyme to confirm the identity of this residue as the catalytic cysteine. The substitution resulted in loss of activity, with no product observed after 1.5 hr incubation in the presence of substrate (see Figure S6). As observed in the structures of *M. sativa* CHS (Ferrer et al., 1999) and *G. hybrida* 2PS (Jez et al., 2000), the electron density at Cys-152 is consistent with the oxidation of this residue into sulfuric acid. Despite considerable efforts, cocrystallization attempts with long- and medium-chain fatty acyl-CoA esters have not been successful. Of note is the fact that ORAS is devoid of any of the positively charged residues that have been observed to line the CoA-binding pockets of other bacterial and plant type III PKSs where they stabilize the charges on the phosphopantetheine. The lack of these stabilizing elements in ORAS may account for the inability to obtain a static binary complex in the time courses required for cocrystallization.

In addition to the active site cysteine (Cys-152) that presents the covalent attachment site necessary for polyketide chain extension (Austin and Noel, 2003; Jez et al., 2001), ORAS also harbors a second cysteine residue (Cys-120) at a position equivalent to that of Cys-106 in *S. coelicolor* THNS (Abe et al., 2005b). In this bacterial enzyme that catalyzes a malonyl-CoA-primed pentaketide formation, Cys-106 is presumed to regulate polyketide reactivity either by facilitating the enolization of the triketide carboxylate, by protonation of the triketide enolate, or by hemithioketal formation during the elongation stage. Site-directed mutagenesis of this cysteine results in derailment of polyketide elongation and in the formation of a triacetic acid lactone (Abe et al., 2005b). The equivalent cysteine in trORAS (Cys-120) was mutated to serine to investigate the role of this residue. The Cys-120→Ser mutant diminished but did not abolish resorcinol production, and the decrease in activity due to this mutation was more pronounced for longer acyl-CoA substrates (Figures S4–S6).

In the structure of trORAS, Cys-120 occupies a position analogous to Thr-132 in *P. sylvestris* stilbene synthase (STS) (Austin et al., 2004a) and *M. sativa* CHS (Ferrer et al., 1999). Prior crystallographic and biochemical analysis demonstrates that the positioning of this residue is critical to the formation of a thioesterase-like hydrogen-bonding network that mediates aldol cyclization specificity (Austin et al., 2004a). This CHS/STS "aldol switch" controls the partitioning of the tetraketide intermediate between two competing chemical paths. Analysis of the active site structure of trORAS reveals that the orientation of Cys-120 is similar to that of Thr-132 in CHS and precludes the formation of a thioesterase-like hydrogen-bonding network for partitioning of intermediates. Consequently, the mechanism for aldol condensation and aromatization by trORAS proceeds through a yet unidentified mechanism distinct from that of STS. In addition, alkylresorcinols are among the products identified for trORAS both in this and in prior studies (Funa et al., 2007; Goyal et al., 2008), suggesting that the stable resorcylic acid is an intermediate that is further enzymatically decarboxylated by ORAS to yield the final alkylresorcinol product. The production of this carboxylated resorcylic acid intermediate by ORAS further distinguishes the mechanism of this enzyme from STS, which does not produce a stilbene carboxylate intermediate (Austin et al., 2004a).

A Reorganized Steric Gate Controls Specificity

Prior biochemical and structural studies on plant and bacterial type III PKSs have established the importance of several residues near the active site in controlling substrate and product specificities, including Thr-197, Gly-256, and Ser-338 of *M. sativa* CHS. In the structure of ORAS, drastic rearrangements at the active site result in significantly deviant dispositions of residues Phe-252 (corresponding to Gly-256) and Met-189 (corresponding to Thr-197) (Figures 3C and 3D). Specifically, the replacement of the smaller side chain of Thr-197 in *M. sativa* CHS with the larger Met-189 in ORAS is compensated by significant expansion of the polypeptide backbone in this region as a result of the α7i helical insertion. Consequently, this substitution actually results in an increase in the active site contour along the backbone at this region. This is in contrast with results obtained for pentaketide chromone synthase (PCS) and octaketide synthase (OKS) from *A. arborescens*, where the residue at the analogous position plays a crucial role in controlling product chain length. Replacement of Gly-207 in OKS with larger side chains results in a smaller active site cavity and alters specificity toward smaller pentaketide products (Abe et al., 2005a), whereas replacement of Met-207 in PCS with smaller side chains (Abe et al., 2005b) increases the active site cavity of this enzyme and alters specificity to larger octaketide products. Surprisingly, mutation of the larger side chain of Met-189 in ORAS with threonine results in significant loss of activity without alterations to the product profile (Figure S8). These data suggest a role for the side chains of Met-189 in orienting substrates in the active site, consistent with the observed binding mode for fatty acids in the trORAS-eicosanoic acid cocrystal structure (see later section for details).

The reorganization of the polypeptide backbone near Met-189 results in a compensatory movement of the flanking β sheet (β9 encompassing residues Leu-250 through Asp-255) into the resultant cavity. In addition, the glycine residue that occupies a critical position along this strand (Gly-256 in *M. sativa* CHS) is replaced with Phe-252 in ORAS, further constricting the walls of the active site along this face of the tunnel (Figures 3C and 3D). As a consequence of these structural reorganizations, Phe-252 is now poised to serve as a steric gate to regulate product specificity, in a manner analogous to the role played by Gly-207 in OKS (Abe et al., 2005a) and Met-207 in PCS (Abe et al., 2005b). Substitution of Phe-252 to glycine in the trORAS enzyme altered the product profile for long-chain acyl-CoA substrates (C_{16} or larger) and specifically disrupted the production of pentaketide resorcinol and resorcylic acid products. With palmitoyl-CoA **5a** (C_{16}) and monounsaturated oleoyl-CoA **6a** (C_{18}) as substrates, minor pentaketide products **5h**, **6g**, and **6h** observed

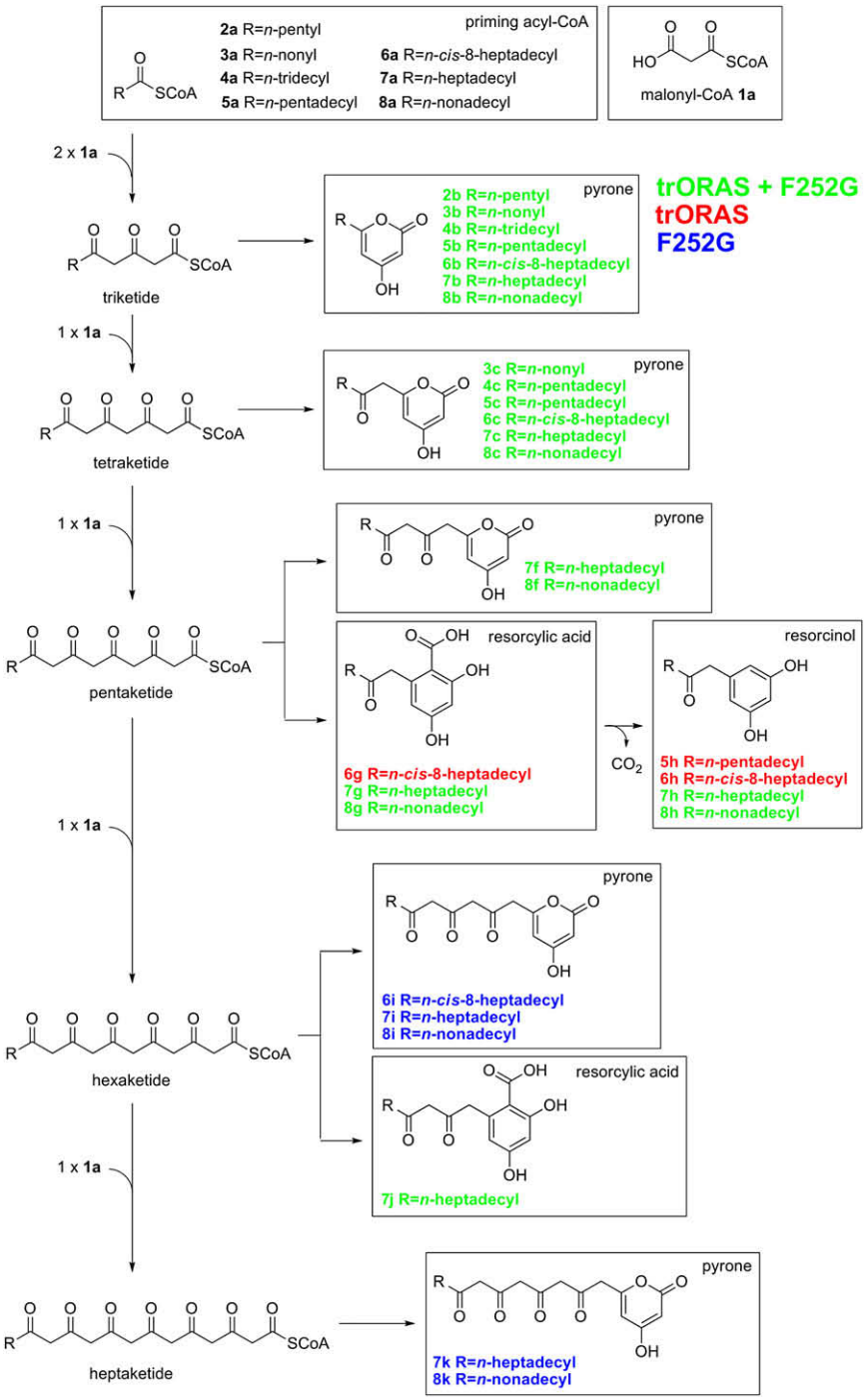

Figure 4. Overview of Reactions Catalyzed by trORAS and the Phe-252→Gly Mutant

Products confirmed by LC-MS/MS for trORAS are shown in red, those for the Phe-252→Gly mutant are shown in blue, and products observed for both enzymes are shown in green. Mass spectral analysis of these products is provided in Table S2.

for the wild-type enzyme were eliminated in the Phe-252→Gly mutant. The effect was most significant for stearoyl-CoA **7a** (C_{18}) and arachidoyl-CoA **8a** (C_{20})-primed reactions, which resulted in increased abundance of pyrone derailment products including hexaketide (**7i**, **8i**) and heptaketide (**7j**, **8j**) pyrones at the expense of the pentaketide resorcinol product (**7h**, **8h**) (Figure 4). Taken together, these results suggest that the length and flexibility of very long (C_{18} and C_{20}) saturated acyl-CoAs allow for extensive interactions along the hydrophobic tunnel of the enzyme, where Phe-252 may play a role in stabilizing the extended linear polyketide chain such that enzymatic resorcinol production will be favored over lactonization in solution.

Structure of the Phe-252→Gly Mutant

In order to confirm that the altered product profile of the Phe-252→Gly mutant is not a consequence of gross structural alterations, the crystal structure of this variant was determined to 2.1 Å resolution, using the coordinates of the unliganded enzyme as a search probe (final R factor/free R factor of 19.8%/25.5%). The overall structure of this variant is almost identical to that of the wild-type enzyme except that unbiased electron density maps clearly show the substitution of Phe-252 by Gly (Figure 5A). Interestingly, clear but discontinuous density can be observed near the active sites in two of the four molecules in the crystallographic asymmetric unit of this variant, and this has been modeled as a molecule of polyethylene glycol (presumably carried over from the crystallization media) (Figure 5A). The larger cavity created in the vicinity of the active site as a consequence of this mutation more easily accommodates the polyethylene glycol, and a similar ligand is also observed in the structure of *S. coelicolor* THNS (Austin et al., 2004b).

The removal of the bulky aromatic side chain from the hydrophobic core of the active site does not compromise packing integrity, and there are minimal perturbations of either of the main-chain atoms as a consequence of the Phe-252→Gly mutation. The rmsd of main-chain atoms between wild-type and Phe-252→Gly trORAS is only 0.2 Å. Whereas the main-chain atoms of wild-type trORAS and the Phe-252→Gly mutant can be accurately superimposed, the side-chain atoms of a number of residues in the vicinity of Gly-252 are altered as a consequence of the mutation. Specifically, the side chains of active site residues Cys-152, Phe-210, Met-189, and a number of additional flanking residues are slightly displaced relative to their positions in the wild-type

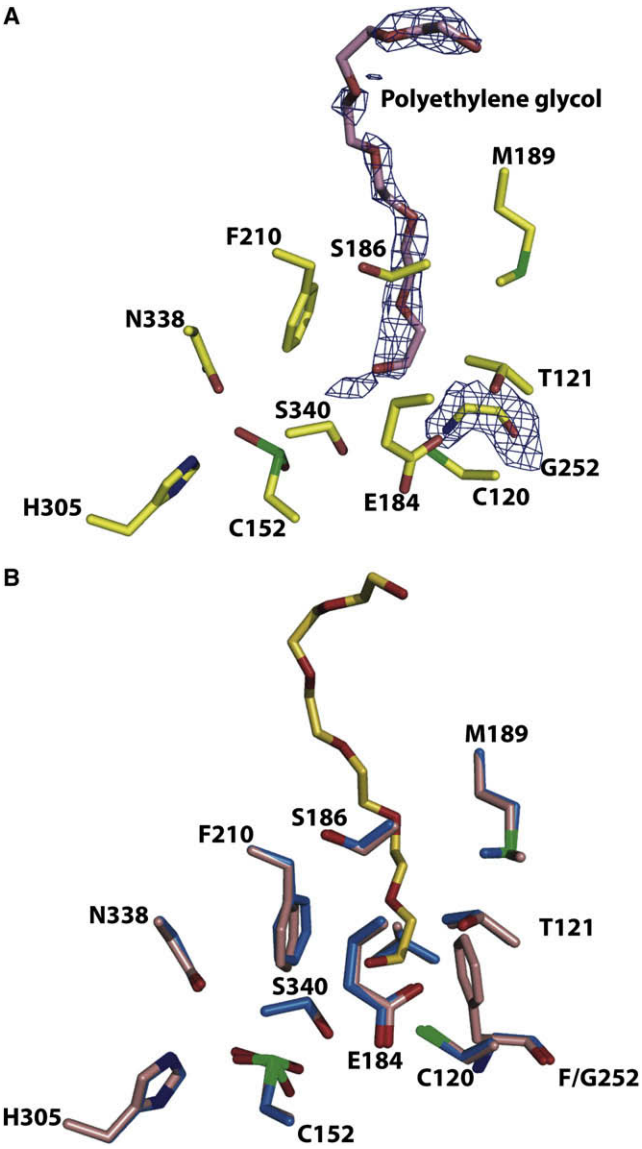

Figure 5. Active Sites of trORAS and the Phe-252→Gly Mutant

(A) Electron density map (shown in blue mesh and contoured at 2.5σ) calculated using Fourier coefficients $F_{obs} - F_{calc}$ with phases derived from the final refined model of Phe-252→Gly trORAS minus the atoms of residue Gly-252 and all active site ligands. Clear, but discontinuous, electron density can be observed near the vicinity of Gly-252 and has been modeled as a molecule of polyethylene glycol. The final refined coordinates of important active site residues are shown as stick figures, the polyethylene glycol is shown in pink. (B) A superposition of active site residues of wild-type trORAS (shown in pink) and the Phe-252→Gly variant (shown in blue). There are no significant changes in the main-chain atoms of the two structures and only small alterations in the position of the active site residues are shown.

trORAS structure (Figure 5B). The lack of any gross structural perturbations as a consequence of the Phe-252→Gly mutation suggests that the derailment of polyketide extension in this variant is a direct consequence of alterations in the activity site cavity, consistent with the role of Phe-252 as a steric regulator of product specificity in ORAS.

A Static Acyl-Binding Tunnel Flanks the Elongation/Extension Site

The active site cavity of ORAS is flanked by an acyl-binding tunnel similar to those observed in the structures of the bacterial type III PKSs *M. tuberculosis* Pks18 and *S. coelicolor* THNS (Austin et al., 2004b; Sankaranarayanan et al., 2004). Although attempts to obtain cocrystals with various CoA esters failed, cocrystallization efforts of trORAS with long-chain fatty acids yielded diffraction-quality crystals, and the structure of a binary complex with eicosanoic acid (a C_{20} fatty acid) has been determined to 2.0 Å resolution by molecular replacement, using the coordinates of the unliganded enzyme as a search probe (final R factor/free R factor of 17.3%/22.5%). Initial, unbiased electron density maps, calculated after a cycle of crystallographic refinement of the molecular replacement solution, revealed strong and continuous electron density corresponding to the entire C_{20} fatty acid in two of the four molecules in the crystallographic asymmetric unit (corresponding to one ligand per biological dimer) (Figures 6A and 6B).

The eicosanoic acid C_{20} fatty acid chain occupies a position similar to that observed for a myristic acid ligand in the structure of *M. tuberculosis* Pks18 (Sankaranarayanan et al., 2004) and a heptamer of polyethylene glycol in the structure of *S. coelicolor* THNS (Austin et al., 2004b) (Figures 6C–6E). In the trORAS cocrystal structure, as in each of the bacterial type III PKSs, the ligand occupies a long acyl-binding tunnel that extends into the "floor" of the PKS active site. However, the carboxyl group of the eicosanoic acid ligand is significantly closer to the two active site cysteines of trORAS (Cys-152 Sγ-O distance of 4.2 Å; and Cys-120 Sγ-O distance of 4.0 Å) than observed for the distance between the ligands and the nucleophilic cysteine in either of the bacterial enzymes (Austin et al., 2004b; Sankaranarayanan et al., 2004). Although the Sγ carboxylate oxygen distances are far too large to suggest covalent linkages, the distance and stereochemical disposition between the carboxyl group of the fatty acid and the two cysteines are consistent with the mechanism of steering polyketide reactivity as suggested by biochemical studies of *S. coelicolor* THNS (Austin et al., 2004b; Sankaranarayanan et al., 2004).

In the trORAS cocrystal structure, the location of the hydrophobic fatty acid tail of the eicosanoic acid ligand is distinct from that observed for ligand complexes of the bacterial type III PKSs (Austin et al., 2004b; Sankaranarayanan et al., 2004). The hydrocarbon tail does not extend out into bulk solvent but rather is directed back inward into the protein and toward the dimer interface (Figures 6C–6E). The trajectory of the hydrocarbon tail is restricted by the α7i helical insertion, which blocks the base of this lower domain of trORAS and guides the ligand back into the protein and away from bulk solvent. A key structural element that orients the hydrocarbon tail is the side chain of Met-189, which forms one side of the wall of the ligand-binding cavity. Mutational analysis demonstrates that replacement of Met-189 with a smaller threonine side chain significantly compromises catalytic activity with smaller-chain acyl-CoAs (Figure S8), consistent with a role of this residue in guiding the binding of hydrocarbon tails of the fatty acid substrates.

During the review process for this manuscript, an independent report of the structure of unliganded ORAS was published by Sankaranarayanan and colleagues (Goyal et al., 2008). Albeit

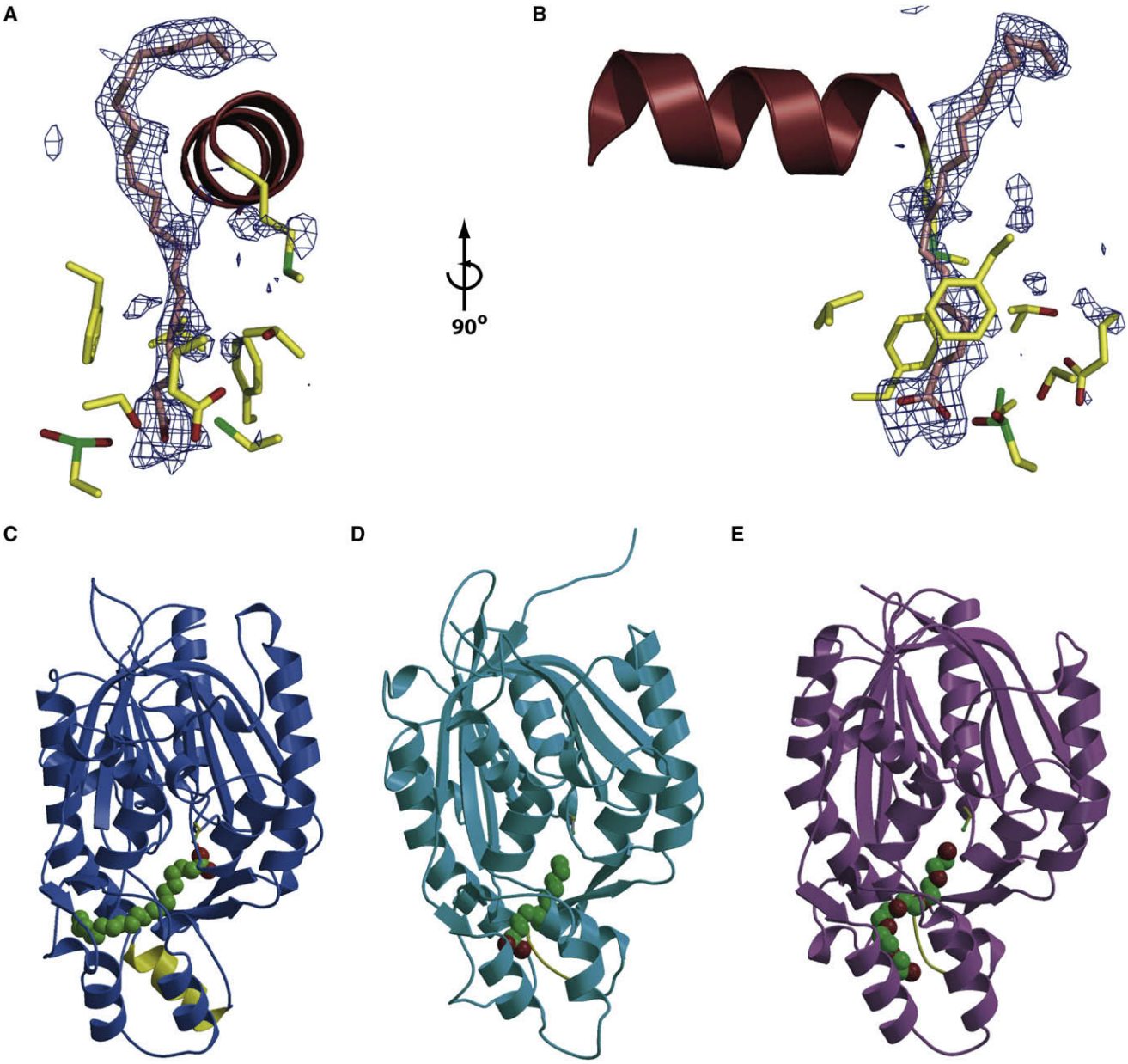

Figure 6. Close-Up View of the Active Site of trORAS Bound to Eicosanoic Acid

(A and B) Orthogonal views of an electron density map (shown in blue mesh and contoured at 2σ) calculated using Fourier coefficients $F_{obs} - F_{calc}$ with phases derived from the final refined model of the ORAS-eicosanoic acid complex minus the atoms of the eicosanoic acid ligand. The final refined coordinates of important active site residues are shown as stick figures, the eicosanonic acid is shown in pink, and the α7 insertion is shown as a ribbon diagram in red.

(C–E) Ribbon diagrams derived from the crystal structures of (C) trORAS (shown in blue) with bound eicosanoic acid, (D) Pks18 (shown in cyan) with bound myristic acid, and (E) THNS (shown in pink) with a bound molecule of polyethylene glycol. Each of the ligands is shown as CPK models and the respective active site cysteine residues are shown in ball-and-stick representation.

of significantly lower resolution, the overall fold of the polypeptide is similar to that detailed in our 1.8 Å resolution structure of trORAS. However, these investigators fail to note the α7i helical insertion that distinguishes the reorganized active site of ORAS from other type III PKSs such as chalcone synthase (Ferrer et al., 1999). In addition, poststructural biochemical analysis carried out by these investigators is based on a model of the fatty acid binding site derived from the structure of the bacterial *M. tuberculosis* Pks18 bound to myristic acid (Sankaranarayanan et al., 2004). However, our 2.0 Å resolution cocrystal structure of trORAS bound to eicosanoic acid reveals that the trajectory of the hydrocarbon tail is distinct from that observed in the Pks18-myristic acid structure, and this novel fatty acid-binding tunnel is created by virtue of the α7i helical insertion (Figures 6C–6E). Consequently, mutational analyses of ORAS based on the Pks18 cocrystal structure are likely not particularly

relevant. It is not surprising that mutations that were designed to sterically occlude the incorrectly identified substrate-binding tunnel (Ser-186→Phe) showed no changes in substrate preference (Goyal et al., 2008). A second double variant (Ser-186→Phe/Ser-340→Leu) was unable to synthesize any products from either short- or long-chain fatty acids (Goyal et al., 2008), and this is likely a consequence of the fact that Ser-340 is immediately adjacent to the catalytic nucleophile (Cys-152) and mutations at this residue will likely interfere with substrate binding regardless of the chain length of the starter unit. The cocrystal structures presented in this current work and the corresponding mutational analyses unambiguously define a unique binding site for the long-chain hydrocarbon tail that distinguishes ORAS from other type III polyketide synthases.

The structures of the unliganded trORAS and the trORAS-eicosanoic acid complex are nearly identical and only small, subtle rearrangements of secondary structural elements along the atoms of the hydrocarbon tail are necessary to accommodate the ligand into the acyl-binding pocket. This is in sharp contrast with studies of *S. coelicolor* THNS and plant type III PKSs that suggest that the acyl-binding tunnel is dynamic and likely undergoes progressive, motional displacement during the extension of the aliphatic tail of polyketide intermediates (Austin et al., 2004b; Austin and Noel, 2003). Particularly noteworthy is the fact that for each of the bacterial type III PKSs that harbors a bound ligand in the acyl-binding pocket, the ligand serendipitously either copurified with protein or was a product of the crystallization medium. No structures of these proteins are available in both the absence and presence of ligand (Austin et al., 2004b; Sankaranarayanan et al., 2004). In contrast, our structure of wild-type unliganded trORAS is devoid of any extraneous ligands, and density for eicosanoic acid is present only when the ligand is explicitly introduced into the crystallization medium. These results have been reinforced by our observations of an unoccupied acyl-binding pocket in structures derived from over two dozen different data sets collected during the course of this work. The presence of a static acyl-binding tunnel may be a unique feature of this fungal type III PKS that distinguishes this enzyme from the bacterial enzymes. Alternatively, a well-defined tunnel may be characteristic of all type III PKS enzymes that utilize long-chain acyl-CoA esters as starter molecules. Further biochemical experiments are currently under way to distinguish between these possibilities.

SIGNIFICANCE

The 2′-oxoalkylresorcylic acid synthase (ORAS) of *N. crassa* is the only known type III polyketide synthase that can produce pentaketide resorcylic acids. The enzyme utilizes a long-chain fatty acid CoA ester starter molecule and carries out sequential condensations with four molecules of malonyl-CoA to yield the resorcylic acid. Our structural analysis of a truncated ORAS mutant reveals a unique rearrangement of secondary structural elements in the lower domain of the enzyme and a reorientation of the gating mechanism for controlling polyketide chain length and cyclization pattern. Similar to bacterial type III polyketide synthases, this fungal enzyme harbors a second active site thiol that may function in the mechanism of steering polyketide reactivity. In the cocrystal structure of trORAS with the C_{20} fatty acid eicosanoic acid, the hydrocarbon tail is accommodated within the protein interior within an extended acyl-binding pocket with a novel trajectory that results from the reorganized lower domain. The structure reveals an unexpected mechanism for sequestering large acyl groups that may be shared among other type III PKSs that utilize long-chain fatty acid CoA esters as starter molecules. These studies establish a framework for further engineering experiments aimed at exploiting the diversity of type III PKSs.

EXPERIMENTAL PROCEDURES

Cloning

A complete listing of primers is given in Table S1. Open reading frame NCU04801.1 (ORAS) was amplified from a library of *N. crassa* mRNA by reverse-transcription PCR in two steps using the First Strand cDNA synthesis kit (Roche Applied Sciences, Mannheim, Germany) and the specific primers FWD1 and REV1, followed by PCR amplification using the same primers. The resulting DNA product was restriction digested and inserted into pET15b to yield pET15b-ORAS. Subsequently, NCU04801.1 was reamplified using the above forward primer and a new reverse primer, REV2, and the resultant PCR product was digested and ligated into pET26b to yield pET26-trORAS. A thrombin protease site was engineered into the reverse primer in order to facilitate cleavage of the carboxy-terminal hexahistidine tag. A carboxy-terminal truncation variant of ORAS (trORAS) was amplified using the above forward primer and the reverse primer REV3, restriction digested, and ligated into pET15b to yield pET15b-trORAS. The DNA sequence of all constructs was verified. DNA sequencing was performed at the University of Illinois Biotechnology Center (Urbana, IL, USA).

Expression and Purification of Recombinant ORAS and trORAS

Plasmids pET26b-ORAS, pET15b-ORAS, and pET15b-trORAS were transformed into *E. coli* BL21 (DE3) and single colonies were used to inoculate 5 ml Luria broth containing 50 μg kanamycin/ml (pET26b) or 100 μg ampicillin/ml (pET15b). Following overnight growth at 37°C, this culture was used to inoculate 500 ml Terrific broth containing the appropriate antibiotic, and grown at 37°C until the optical density at 600 nm reached 0.8. Protein expression was induced with the addition of 0.25 mM isopropyl-β-D-thiogalactopyranoside (IPTG), and growth was continued for an additional 18 hr at 25°C. The flasks were chilled for 30 min, and then the cells were harvested by centrifugation (6000 × g, 4°C, 15 min). The resulting pellet was resuspended in 2 ml lysis buffer (10 mM imidazole, 50 mM sodium phosphate buffer, 300 mM NaCl, 15% glycerol [pH 8.0], 1 mg/ml lysozyme) per gram cell weight and frozen at −80°C. Subsequently, cells were lysed using a French press and cellular debris was removed by centrifugation (40,000 × g, 4°C, 10 min, twice). Recombinant proteins were purified by chromatography on Ni-NTA resin by virtue of the engineered carboxy-terminal (wild-type ORAS) or amino-terminal (trORAS) hexahistidine affinity tag. Captured protein was washed with wash buffers (20, 30, and 50 mM imidazole, 50 mM sodium phosphate buffer, 300 mM NaCl, 15% glycerol [pH 8.0]) and finally eluted in elution buffer (100 mM imidazole, 50 mM sodium phosphate buffer, 300 mM NaCl, 15% glycerol [pH 8.0]). The protein content of individual elution fractions was estimated using the Quick Start Bradford protein assay (Bio-Rad, Hercules, CA, USA) and the appropriate fractions were pooled and buffer exchanged into 10 mM MOPS buffer (pH 7.5) containing 15% glycerol overnight at 4°C. The protein was concentrated using an Amicon ultracentrifugal filter device (Millipore, Billerica, MA, USA). Representative SDS-PAGE analysis of recombinant protein is shown in Figure S2. The hexahistidine tags were removed using the Thrombin Cleavage Capture kit (Novagen, Madison, WI).

Determination of Kinetic Parameters

Experiments to determine the kinetic parameters of wild-type and truncated ORAS enzyme with stearoyl-CoA were carried out in triplicate. Experiments were conducted according to the method of Funa et al. (2007) with some modifications. Each reaction contained 50 mM Tris-HCl (pH 7.0), 0.5 μM

recombinant protein (ORAS or trORAS), and 100 mM malonyl-CoA in a total reaction volume of 400 μl. The concentration of priming acyl-CoA was varied between 0.5 and 10 μM stearoyl-CoA. Reaction mixtures were preincubated at 30°C for 4 min before addition of malonyl-CoA. After mixing, a 100 μl aliquot of the reaction was removed and stopped immediately by addition of 20 μl of a solution of 4% trifluoroacetic acid in water. Subsequently, a second aliquot was removed at 45 s and quenched by the same method. Samples were kept at 4°C until analysis by HPLC. The reactions were analyzed using an Agilent 1100 Series HPLC and ZORBAX SB-C_{18} reverse-phase column (3.0 × 150 mm, 3.5 μm) (Agilent Technologies, Palo Alto, CA, USA) monitoring at 258 nm, with conditions as follows: 0.5 ml/min; 25°C; solvent A: 15 mM ammonium formate; solvent B: 90% methanol, 10% 10 mM ammonium acetate (pH 7.3), adjusted using acetic acid; 0–15 min, 5%–20% B, 15–20 min, 20%–100% B, 20–27 min, 100% B. Peaks at 7 min and 9.5 min corresponded to authentic malonyl-CoA and CoASH, respectively. The initial rates of CoASH production determined from these reactions were fitted to the Michaelis-Menten equation using nonlinear least-squares regression analysis in Microcal Origin 5.0 (Microcal Software, Northampton, MA, USA) to calculate k_{cat} and K_M.

Preparation of ORAS Mutants and Product Profile Analysis

Site-directed mutants were created using the QuikChange Site-Directed Mutagenesis kit (Stratagene, La Jolla, CA, USA). From the pET15b-trORAS plasmid, the primers 252-F and 252-R were used to generate the Phe-252→Gly mutant, 152-F and 152-R were used to generate the Cys-152→Thr mutant, and 120-F and 120-R were used to generate the Cys-120→Ser mutant. The DNA sequence of each mutant was verified and the mutants were expressed by the same method as described for ORAS and trORAS. Reactions for product profile analysis contained 50 mM Tris-HCl (pH 7.0), 4 μM recombinant protein (ORAS, trORAS, or mutant), and the concentration of priming acyl-CoA and malonyl-CoA was 200 μM in a total reaction volume of 250 μl. Reaction mixtures were incubated at 30°C for 1.5 hr followed by HPLC analysis as described in Supplemental Experimental Procedures. The polyketide products were characterized by liquid chromatography-quadrupole time-of-flight mass spectrometry on a Micromass Q-Tof Ultima (Waters, Milford, MA, USA). Mass spectrometry was performed at the University of Illinois Mass Spectrometry Laboratory (Urbana, IL, USA).

Crystallization

For crystallization efforts, truncated ORAS (trORAS) and the Phe-252→Gly mutant of truncated ORAS were purified as described above, and its amino-terminal polyhistidine tag was removed using thrombin (1 U/mg protein; GE Healthcare, Piscataway, NJ, USA). The protein was further purified by anion-exchange (5 ml HiTrap Q; GE Healthcare) and size-exclusion chromatographies (Superdex 75 16/60; GE Healthcare). Selenomethionine-incorporated trORAS (SeMet trORAS) was produced by the method of van Duyne et al. (1993) and purified as described, except that 5 mM DTT was included in all of the buffers.

Crystals of native and SeMet trORAS and the Phe-252→Gly mutant were grown by the hanging-drop vapor-diffusion method. In each case, 1.5 μl protein (5 mg/ml) was mixed with 1.5 μl precipitant solution containing 18% polyethylene glycol 8000, 100 mM HEPES (pH 7.5), with 1% polyethylene glycol 3350 as an additive. The mixture drop was equilibrated over a well containing the same precipitant solution at 20°C, and crystals reached their maximum size after 3 days. Crystals that diffracted to slightly higher resolutions could be produced by incubation at 4°C, but these crystals took several weeks to grow and were not easily reproduced. Hence, initial phase determination utilized crystals grown at 20°C and subsequent crystallographic refinement was conducted against data collected from a crystal grown at 4°C. Crystals were briefly immersed in a solution consisting of the crystallization liquor supplemented with 25% glycerol, prior to vitrification by immersion in liquid nitrogen. For crystallization of ligand complexes, the appropriate ligand was added to the protein to a final concentration of 2–5 mM prior to crystallization.

Phasing and Structure Determination

A four-fold redundant data set was collected from orthorhombic crystals of selenomethionine-substituted trORAS at the selenium absorption edge, to a limiting resolution of 2.0 Å (overall R_{merge} = 8.6, I/σ (I) = 2.4 in the highest resolution shell) utilizing a Mar 300 CCD detector (LS-CAT, Sector 21 ID-D, Advanced Photon Source, Argonne, IL, USA). The structure of trORAS was solved by single-wavelength anomalous diffraction utilizing anomalous scattering from the 14 selenium-substituted methionine residues per monomer. Data were indexed and scaled using the HKL2000 package (Otwinowski et al., 2003). Selenium sites were identified using HySS (Grosse-Kunstleve and Adams, 2003) and the heavy-atom substructure was imported to SHARP (Bricogne, et al., 2003) for maximum-likelihood refinement and phase calculation, yielding an initial figure of merit of 0.425 to 2.2 Å resolution. Solvent flattening using DM (Cowtan and Main, 1998) further improved the quality of the initial map (solvent-flattened figure of merit = 0.696). The resultant electron density map was of exceptional quality and permitted most of the main-chain and 75% of side-chain residues to be automatically built using ARP/wARP (Perrakis et al., 1997). The remainder of the model was fitted using XtalView (McRee, 1999) and further improved by rounds of refinement with REFMAC5 (Murshudov et al., 1997, 1999) and manual building. Subsequent rounds of model building and crystallographic refinement utilized data from a crystal of trORAS grown under similar conditions at 4°C that diffracted to 1.75 Å resolution (overall R_{merge} = 7.7, I/σ [I] = 4.8 in the highest resolution shell). Crossvalidation, using 5%–7% of the data for the calculation of the free R factor, was utilized throughout the model-building process in order to monitor building bias (Kleywegt and Brunger, 1996).

Crystals of Phe-252→Gly trORAS occupy a monoclinic setting. A three-fold redundant data set was collected to a resolution limit of 2.1 Å (overall R_{merge} = 7.1, I/σ [I] = 2.8 in the highest resolution shell) utilizing a Mar 225 CCD detector. The structure of Phe-252→Gly trORAS was determined to 2.1 Å resolution by molecular replacement using the refined coordinates of unliganded ORAS structure as a search probe. Multiple rounds of manual model building using XtalView (McRee, 1999) were interspersed with refinement using REFMAC5 (Murshudov et al., 1997, 1999) to complete structure refinement. Crossvalidation used 5% of the data in the calculation of the free R factor.

Crystals of the trORAS-eicosanoic acid complex also occupy a monoclinic setting. A four-fold redundant data set of the complex was collected to a Bragg limit of 2.0 Å (overall R_{merge} = 8.1, I/σ [I] = 3.9 in the highest resolution shell) utilizing a Mar 300 CCD detector. The structure of the trORAS-eicosanoic acid complex was determined to 2.0 Å resolution by molecular replacement using the refined coordinates of the unliganded trORAS structure as a search probe. Multiple rounds of manual model building using XtalView (McRee, 1999) were interspersed with refinement using REFMAC5 (Murshudov et al., 1997, 1999) to complete structure refinement. The eicosanoic acid ligand was manually built into the difference Fourier maps after the free R factor dropped below 30%. Crossvalidation used 5% of the data in the calculation of the free R factor.

For each of the structures, stereochemistry of the model was monitored throughout the course of refinement using PROCHECK (Laskowski et al., 1996). Crystal parameters, data collection parameters, and refinement statistics for each of the structures are summarized in Table 1.

ACCESSION NUMBERS

Coordinates have been deposited in the Protein Data Bank with accession codes 3EUO (Native ORAS), 3EUQ (ORAS F252G mutant), and 3EUT (ORAS-eicosanoic acid complex).

SUPPLEMENTAL DATA

Supplemental Data include eight figures, two tables, Supplemental Experimental Procedures, and Supplemental References and can be found with this article online at http://www.chembiol.com/cgi/content/full/15/10/1079/DC1/.

ACKNOWLEDGMENTS

This research was supported by a grant from the Office of Naval Research (N00014-02-1-0725 to H.Z.) and NIGMS (S.K.N.). We thank John Chrzas and staff at SER-CAT (22-BM at Argonne National Laboratories) for facilitating data collection. We thank N. Nair for preparation of the *Neurospora crassa*

mRNA library and Anuradha Biswas for assistance in protein purification. S.B.R.-P. acknowledges support from the National Institutes of Health Cell and Molecular Biology Training Grant Program and the National Science Foundation Graduate Research Fellowship Program. The Q-Tof Ultima mass spectrometer was purchased in part with a grant from the National Science Foundation, Division of Biological Infrastructure (DBI-0100085). The authors declare that they have no competing interests.

Received: April 7, 2008
Revised: July 24, 2008
Accepted: August 8, 2008
Published: October 17, 2008

REFERENCES

Abe, I., Oguro, S., Utsumi, Y., Sano, Y., and Noguchi, H. (2005a). Engineered biosynthesis of plant polyketides: chain length control in an octaketide-producing plant type III polyketide synthase. J. Am. Chem. Soc. *127*, 12709–12716.

Abe, I., Utsumi, Y., Oguro, S., Morita, H., Sano, Y., and Noguchi, H. (2005b). A plant type III polyketide synthase that produces pentaketide chromone. J. Am. Chem. Soc. *127*, 1362–1363.

Austin, M.B., and Noel, J.P. (2003). The chalcone synthase superfamily of type III polyketide synthases. Nat. Prod. Rep. *20*, 79–110.

Austin, M.B., Bowman, M.E., Ferrer, J.L., Schroder, J., and Noel, J.P. (2004a). An aldol switch discovered in stilbene synthases mediates cyclization specificity of type III polyketide synthases. Chem. Biol. *11*, 1179–1194.

Austin, M.B., Izumikawa, M., Bowman, M.E., Udwary, D.W., Ferrer, J.L., Moore, B.S., and Noel, J.P. (2004b). Crystal structure of a bacterial type III polyketide synthase and enzymatic control of reactive polyketide intermediates. J. Biol. Chem. *279*, 45162–45174.

Berman, H.M., Westbrook, J., Feng, Z., Gilliland, G., Bhat, T.N., Weissig, H., Shindyalov, I.N., and Bourne, P.E. (2000). The Protein Data Bank. Nucleic Acids Res. *28*, 235–242.

Bricogne, G., Vonrhein, C., Flensburg, C., Schiltz, M., and Paciorek, W. (2003). Generation, representation and flow of phase information in structure determination: recent developments in and around SHARP 2.0. Acta Crystallogr. D Biol. Crystallogr. *59*, 2023–2030.

Cowtan, K., and Main, P. (1998). Miscellaneous algorithms for density modification. Acta Crystallogr. D Biol. Crystallogr. *54*, 487–493.

Cox, R. (2007). Polyketides, proteins and genes in fungi: programmed nanomachines begin to reveal their secrets. Org. Biomol. Chem. *7*, 2010–2026.

Ferrer, J.L., Jez, J.M., Bowman, M.E., Dixon, R.A., and Noel, J.P. (1999). Structure of chalcone synthase and the molecular basis of plant polyketide biosynthesis. Nat. Struct. Biol. *6*, 775–784.

Funa, N., Awakawa, T., and Horinouchi, S. (2007). Pentaketide resorcylic acid synthesis by type III polyketide synthase from *Neurospora crassa*. J. Biol. Chem. *282*, 14476–14481.

Goyal, A., Saxena, P., Rahman, A., Singh, P.K., Kasbekar, D.P., Gokhale, R.S., and Sankaranarayanan, R. (2008). Structural insights into biosynthesis of resorcinolic lipids by a type III polyketide synthase in *Neurospora crassa*. J. Struct. Biol. *162*, 411–421.

Grosse-Kunstleve, R.W., and Adams, P.D. (2003). Substructure search procedures for macromolecular structures. Acta Crystallogr. D Biol. Crystallogr. *59*, 1966–1973.

Holm, L., and Sander, C. (1995). Dali: a network tool for protein structure comparison. Trends Biochem. Sci. *20*, 478–480.

Izumikawa, M., Shipley, P.R., Hopke, J.N., O'Hare, T., Xiang, L., Noel, J.P., and Moore, B.S. (2003). Expression and characterization of the type III polyketide synthase 1,3,6,8-tetrahydroxynaphthalene synthase from *Streptomyces coelicolor* A3(2). J. Ind. Microbiol. Biotechnol. *30*, 510–515.

Jez, J.M., Austin, M.B., Ferrer, J., Bowman, M.E., Schroder, J., and Noel, J.P. (2000). Structural control of polyketide formation in plant-specific polyketide synthases. Chem. Biol. *7*, 919–930.

Jez, J.M., Ferrer, J.L., Bowman, M.E., Austin, M.B., Schroder, J., Dixon, R.A., and Noel, J.P. (2001). Structure and mechanism of chalcone synthase-like polyketide synthases. J. Ind. Microbiol. Biotechnol. *27*, 393–398.

Kleywegt, G.J., and Brunger, A.T. (1996). Checking your imagination: applications of the free R value. Structure *4*, 897–904.

Laskowski, R.A., Rullmannn, J.A., MacArthur, M.W., Kaptein, R., and Thornton, J.M. (1996). AQUA and PROCHECK-NMR: programs for checking the quality of protein structures solved by NMR. J. Biomol. NMR *8*, 477–486.

McRee, D.E. (1999). XtalView/Xfit—a versatile program for manipulating atomic coordinates and electron density. J. Struct. Biol. *125*, 156–165.

Morita, H., Kondo, S., Oguro, S., Noguchi, H., Sugio, S., Abe, I., and Kohno, T. (2007). Structural insight into chain-length control and product specificity of pentaketide chromone synthase from *Aloe arborescens*. Chem. Biol. *14*, 359–369.

Murshudov, G.N., Vagin, A.A., and Dodson, E.J. (1997). Refinement of macromolecular structures by the maximum-likelihood method. Acta Crystallogr. D Biol. Crystallogr. *53*, 240–255.

Murshudov, G.N., Vagin, A.A., Lebedev, A., Wilson, K.S., and Dodson, E.J. (1999). Efficient anisotropic refinement of macromolecular structures using FFT. Acta Crystallogr. D Biol. Crystallogr. *55*, 247–255.

Otwinowski, Z., Borek, D., Majewski, W., and Minor, W. (2003). Multiparametric scaling of diffraction intensities. Acta Crystallogr. A *59*, 228–234.

Perrakis, A., Sixma, T.K., Wilson, K.S., and Lamzin, V.S. (1997). wARP: improvement and extension of crystallographic phases by weighted averaging of multiple-refined dummy atomic models. Acta Crystallogr. D Biol. Crystallogr. *53*, 448–455.

Sankaranarayanan, R., Saxena, P., Marathe, U.B., Gokhale, R.S., Shanmugam, V.M., and Rukmini, R. (2004). A novel tunnel in mycobacterial type III polyketide synthase reveals the structural basis for generating diverse metabolites. Nat. Struct. Mol. Biol. *11*, 894–900.

Schröder, J. (1999). Probing plant polyketide biosynthesis. Nat. Struct. Biol. *6*, 714–716.

Seshime, Y., Juvvadi, P.R., Fujii, I., and Kitamoto, K. (2005). Discovery of a novel superfamily of type III polyketide synthases in *Aspergillus oryzae*. Biochem. Biophys. Res. Commun. *331*, 253–260.

van Duyne, G.D., Standaert, R.F., Karplus, P.A., Schreiber, S.L., and Clardy, J. (1993). Atomic structures of the human immunophilin FKBP-12 complexes with FK506 and rapamycin. J. Mol. Biol. *229*, 105–124.

Watanabe, K., Praseuth, A.P., and Wang, C.C. (2007). A comprehensive and engaging overview of the type III family of polyketide synthases. Curr. Opin. Chem. Biol. *11*, 279–286.

